

Contribution of microtubule growth polarity and flux to spindle assembly and functioning in plant cells

Pankaj Dhonukshe^{*‡}, Norbert Vischer and Theodorus W. J. Gadella Jr[‡]

Section of Molecular Cytology and Centre for Advanced Microscopy, Swammerdam Institute for Life Sciences, University of Amsterdam, Kruislaan 316, 1098 SM Amsterdam, The Netherlands

^{*}Present address: Centre for Plant Molecular Biology (ZMBP), University of Tübingen, Auf der Morgenstelle 3, 72076 Tübingen, Germany

[‡]Authors for correspondence (e-mail: pankaj.dhonukshe@zmbp.uni-tuebingen.de; gadella@science.uva.nl)

Accepted 15 May 2006

Journal of Cell Science 119, 3193-3205 Published by The Company of Biologists 2006

doi:10.1242/jcs.03048

Summary

The spindle occupies a central position in cell division as it builds up the chromosome-separating machine. Here we analysed the dynamics of spindle formation in acentrosomal plant cells by visualizing microtubules labelled with GFP-EB1, GFP-MAP4 and GFP- α -tubulin and chromosomes marked by the vital dye SYTO82. During prophase, few microtubules penetrate the nuclear area, followed by nuclear envelope disintegration. During prometaphase, microtubules invading the nuclear space develop a spindle axis from few bipolar microtubule bundles, which is followed by spindle assembly. Using a novel quantitative kymograph analysis based on Fourier transformation, we measured the microtubule growth trajectories of the entire dynamic metaphase spindle. Microtubules initiating from spindle poles either pass through the metaphase plate to form interpolar microtubule bundles or grow until they reach

chromosomes. We also noticed a minor fraction of microtubules growing away from the chromosomes. Microtubules grow at 10 $\mu\text{m}/\text{minute}$ both at the spindle equator and at the spindle poles. Photobleached marks created on metaphase and anaphase spindles revealed a poleward tubulin flux. During anaphase, the velocity of tubulin flux (2 $\mu\text{m}/\text{minute}$) equals the speed of chromatid-separation. With these findings we identified spatially coordinated microtubule growth dynamics and microtubule flux-based chromosome-separation as important facets of plant spindle operation.

Supplementary material available online at <http://jcs.biologists.org/cgi/content/full/119/15/3193/DC1>

Key words: Spindle, GFP, Microtubule, Flux, EB1

Introduction

Cell division involving equal distribution of the duplicated genome is an essential feature of life. In eukaryotes, a specialized microtubular structure, the spindle, takes care of this fundamental process. The spindle assembles by forming a bipolar antiparallel microtubule array that separates the duplicated chromosomes with a stunning precision. During the last three decades many mechanistic models were proposed for spindle formation, two of which dominate the current debate (Karsenti and Vernos, 2001; Mitchison and Salmon, 2001). In the first model, known as the 'search and capture' model (Kirschner and Mitchison, 1986), centrosomes are the central players for the spindle assembly in which highly dynamic microtubules nucleated by the two centrosomes are captured and stabilized by kinetochores on chromosomes leading to bipolar spindle formation. This pathway of spindle formation seems to be dominant in mammalian mitotic spindles (possessing centrosomes), and in fungal mitotic and meiotic spindles (containing the centrosomal counterpart spindle pole bodies). By contrast, in the second model, called the 'distance' model (Karsenti and Vernos, 2001), the chromosomes become the source of spindle organization either by initiating microtubules near them (Carazo-Salas et al., 1999; Heald et al., 1996), or by attracting the astral microtubules by long range interaction to participate in spindle formation (Carazo-Salas

and Karsenti, 2003). This self-organization pathway remains dominant in spindles that lack well-defined microtubule organizing centres (MTOCs), such as the oocyte meiotic spindles in insects and vertebrates (Matthies et al., 1996; Karsenti and Vernos, 2001) and even in some cells possessing centrosomes (Maiato et al., 2004). The two pathways are not mutually exclusive for achieving bipolarity, as laser ablation (Khodjakov et al., 2000), genetic perturbation (Bonaccorsi et al., 1998) or displacement of centrosomes (Rebollo et al., 2004), as well as the absence of kinetochores (Heald et al., 1996) all induce the self-assembly pathway for spindle formation in normal centrosome dominated systems.

Apart from spindle assembly, accurate chromosomal segregation is also important. Separation of sister chromatids involves both chromosome-to-pole movement (anaphase A) and spindle pole-to-pole elongation (anaphase B) (Sharp et al., 2000). For anaphase A, two mechanisms exist. The pacman mechanism, involves kinetochore-associated-motors that work in concert with the microtubule plus end disassembly to actively pull chromatids towards the pole. Alternatively, according to the traction fibre model the poleward translocation (flux) of the entire spindle microtubule lattice, including attached chromatids (in conjugation with the microtubule minus end disassembly at spindle poles) operates to separate chromatids (Mitchison and Salmon, 2001). For anaphase B, the

spindle pole-to-pole distance is increased by the sliding of overlap microtubules at the spindle equator, pushing the poles apart, and by outward forces exerted by the astral microtubules growing away from the poles towards the cell cortex for pulling the poles apart.

Besides the action of motor proteins exerting force between microtubule structures, also dynamic microtubule events contribute to force generation and movement. For instance microtubules can polymerize at the growing end (or plus end) pushing structures forward. Plus ends of microtubules can be visualized (also in living plant cells) using microtubule plus end binding proteins such as EB1 or CLIP170 attached to a GFP-label (Chan et al., 2003; Dhonukshe and Gadella, Jr, 2003; Mathur et al., 2003; Dhonukshe et al., 2005). While growing at the plus end, microtubules can simultaneously depolymerise at their minus ends; this is called microtubule treadmilling. In microtubule treadmilling [also observed in plants (Shaw et al., 2003)], tubulin subunits are added to the microtubule plus end and removed from the minus end with an apparent translocation of the entire structure in the plus end direction (similar to caterpillar-equipped vehicles). By contrast, in the case of microtubule flux, the polymer itself is continuously transported in the direction of its minus end (i.e. towards the spindle pole) with removal of the tubulin subunits from its minus end together with addition of tubulin subunits from its plus end (Mitchison, 1989; Maddox et al., 2002). Microtubule flux is a major component of spindle dynamics in *Xenopus* egg extracts and intact Crane Fly male meiotic cells that do not show metaphase oscillations of chromosomes (Desai et al., 1998; LaFountain et al., 2001) while it does not occur in yeast spindles (Maddox et al., 2000).

Cell wall-encased plant cells do not contain discrete MTOCs (Marc, 1997) but still display well-organized cell-cycle-dependent microtubular arrays, including the spindle. During interphase, plant microtubules mainly remain underneath the cortex (Ledbetter and Porter, 1963) from where they organize around the nucleus, at the onset of mitosis, to generate bipolar spindles with less focused spindle poles (Smirnova and Bajer, 1992). Sophisticated real-time fluorescence microscopy techniques coupled to genetically encoded labelling strategies and the availability of single cell and in vitro systems, enabled the detailed analysis of spindle formation and functioning in non-plant systems (Rieder and Khodjakov, 2003). Recently, GFP-labelled EB1 was used in a study of spindles formed in transiently transfected *Arabidopsis* suspension cells (Chan et al., 2005) with a proposal of different pathways for spindle formation. Here we applied detailed and quantitative real-time fluorescence microscopy for investigating spindle assembly and chromosome separation in much better defined stable transformed BY2-suspension cell system. Our high-resolution spindle imaging allowed, for the first time, the quantification of individual microtubule growth events in the highly crowded plant mitotic spindle. Our results suggest that microtubules puncturing the nuclear envelope (NE) invade the nuclear space during prophase. Subsequently, the bipolar spindle emerges from several antiparallel microtubule bundles defining the spindle axis. During metaphase, microtubules grow mainly from the spindle pole towards the chromosomes but partially also in the other direction, all at a speed of $\sim 10 \mu\text{m}/\text{minutes}$. By creating photobleached marks on GFP- α tubulin-labelled spindles, we identified poleward tubulin flux operating at a

speed of $\sim 2 \mu\text{m}/\text{minute}$ during both metaphase and anaphase. Strikingly, the rate of microtubule flux equals the pace of chromatid separation. We have discussed the implications of these findings in terms of the chromosomal pathway for spindle assembly and a microtubule flux-based mechanism for anaphase progression in acentrosomal plant cells.

Results

Microtubules penetrate the NE followed by its rupture for subsequent spindle assembly

Tobacco BY-2 cells provide an excellent single cell plant system for performing time-lapse fluorescence microscopy as they do not autofluoresce, they divide continuously with a relatively short cell cycle time and they are easily transformable with GFP-based reporter genes (Geelen and Inze, 2001). For analyzing microtubule dynamics during spindle formation we used GFP-MAP4, which labels entire microtubules (Dhonukshe and Gadella, 2003), GFP-*Arabidopsis* α tubulin 6 (GFP-TUA6), which incorporates into entire microtubules (Dhonukshe and Gadella, 2003; Ueda et al., 1999) and GFP-*Arabidopsis* EB1 (GFP-AtEB1), which labels the microtubule plus ends (Mathur et al., 2003; Dhonukshe et al., 2005). We stably transformed BY-2 cells with these reporters driven under the control of the constitutive 35S promoter. To minimize the effect, if any, of 35S promoter based reporter overexpression, we selected transformed cell lines that appeared similar to controls and showed detectable levels of GFP fluorescence. Furthermore, we determined whether they grow and divide normally by analyzing their growth characteristics. The cell lines under investigation exhibited sigmoidal growth curves similar to controls as inferred from the relative cell density profiles (Dhonukshe and Gadella, 2003) of weekly subcultured cells (supplementary material Fig. S1A), which suggests that the expression of GFP-AtEB1 and GFP-TUA6 do not affect mitosis.

We first confirmed the GFP-AtEB1 labelling pattern to plant microtubules in BY-2 cells by co-visualizing it with YFP-MAP4 (Dhonukshe et al., 2005). GFP-AtEB1 'comets' specifically decorated the growing ends of YFP-MAP4-labelled microtubules and they were lost from the microtubules immediately after microtubules started shrinking (supplementary material Fig. S1B-F) (Dhonukshe et al., 2005). In support, a previous study in *Arabidopsis* suspension cells using 35S promoter has shown plus-end-specific localization of AtEB1 by the saw teeth appearance of the growth curves in which AtEB1 remains mainly on the growing ends and not on the shrinking ends (Chan et al., 2003). Furthermore, a recent promoter analysis testing the endogenous AtEB1 promoter and an inducible heat shock promoter revealed that GFP-AtEB1 localization was mainly restricted to the comet-shaped structures at growing microtubule ends (Bisgrove et al., 2004), which was similar to our observations and confirmed that the expression of AtEB1 under the control of the 35S promoter does not affect its microtubular labelling.

We observed microtubule dynamics during G2-M transition by confocal scanning of GFP-MAP4 and GFP-AtEB1 cells and analyzed the cells that remained in focus for the whole scanning duration. At later stages of preprophase, with the narrowing of the preprophase band (PPB) and the nucleus being well positioned at the cell centre, GFP-MAP4 exhibited intense labelling on the NE, which indicates a large

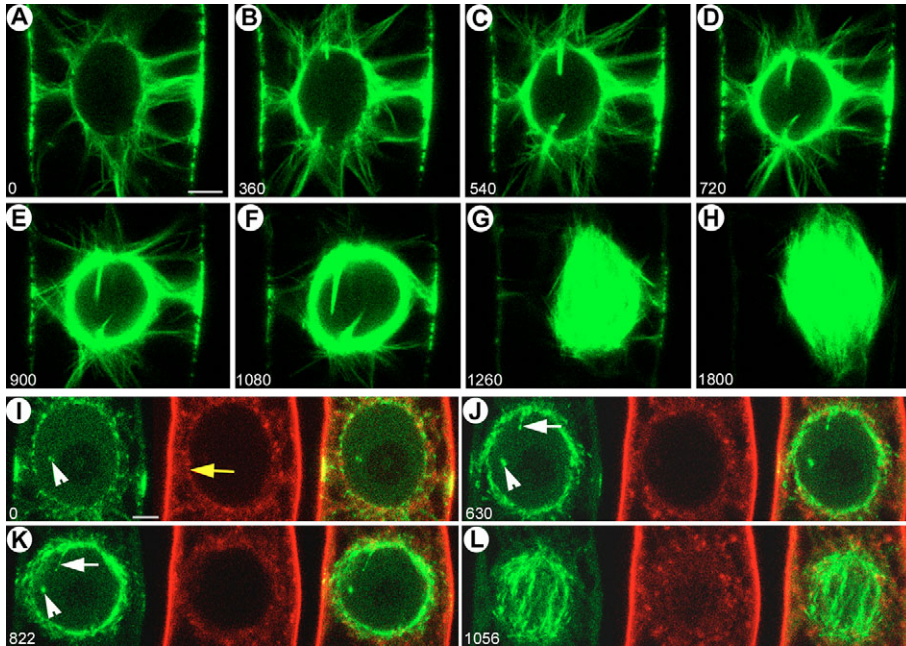


Fig. 1. Microtubule dynamics during NE breakdown. (A-H) Gradual appearance of GFP-MAP4-labelled microtubules around the NE before its disintegration. Note the GFP-MAP4-labelled microtubules penetrate inside the NE before spindle initiation (image C-F). (I-L) Dynamics of GFP-AtEB1-labelled microtubule plus ends during NE breakdown. Microtubule plus ends are in green and FM4-64-labelled endocytic vesicles are in red. White arrows indicate plus ends of microtubules penetrating inside NE from the polar region; white arrowheads indicate plus ends of microtubules penetrating inside NE in a direction perpendicular to the confocal section; the yellow arrow indicates integrity of the NE. Note the appearance of GFP-AtEB1 inside the NE by microtubule penetrations and the continuity of NE integrity as revealed by the persistence of endocytic vesicles outside the nuclear area until significant NE breakdown. Bars, 5 μm ; time is indicated in seconds.

accumulation of microtubules (Fig. 1A-F) (see also Dhonukshe et al., 2003). At the onset of prometaphase, GFP-MAP4-labelled microtubules penetrated the NE (Fig. 1B-F) and similar penetrations were observed with GFP-AtEB1 labelling (Fig. 1J,K). In order to investigate whether the microtubule penetrations induced rupture of the NE, we labelled the cells with the membrane dye FM4-64. FM4-64 has been used as an endocytic tracer in plant cells as it mainly labels endosomes within the first 2 hours after its administration (Emans et al., 2002; Dhonukshe et al., 2005; Dhonukshe et al., 2006). In interphase cells with the NE still intact, FM4-64 remains in cytosolic endosomal vesicles that are excluded from the nucleus. Co-visualization of GFP-AtEB1 and FM4-64 during preprophase revealed microtubule penetration inside the NE before FM4-64-labelled endosomes flooded the nuclear space (Fig. 1I-K). Only a few minutes later, the FM4-64-labelled endosomes entered the nuclear area (Fig. 1L). In addition, the remains of the PPB persisted until spindle initiation (Fig. 1G). Apparently, the NE is first permeable to microtubules and only after NE-breakdown, the nuclear area becomes accessible to larger structures such as endocytic vesicles. These results could indicate a gradual NE-disintegration process, but also could suggest that microtubule-punctures are instrumental for enhancing NE-disintegration as shown previously for mammalian cells (Beaudouin et al., 2002).

To investigate the contribution of the chromosomes in the spindle initiation-process, we either used the vital DNA stain SYTO82 (Fig. 2L-U) or observed chromosomes in negative stain (Fig. 2A-J). During prophase, the intact nucleolus could be clearly seen (yellow arrow in Fig. 2M), and SYTO82-labelled chromosomes appeared near the NE (Fig. 2L,M). Clearly, upon growth of microtubules penetrating the NE, the GFP-AtEB1-labelled microtubule plus ends can come very close to SYTO82-labelled chromosomes in the nuclear area (Fig. 2L,M, white arrowheads). Sometimes, microtubule growth appeared as foci within close proximity of SYTO82-labelled chromosomes (Fig. 2N-Q). About a minute after the

appearance of these foci, the number of GFP-AtEB1-labelled microtubule plus ends inside the nucleus increased (Fig. 2C,R). Within a few seconds, concomitantly with the apparent NE disintegration (and nucleolus disappearance), chromosomes moved to the central area of the former nucleus and the great mass of microtubules already present around NE rapidly occupied the former nuclear region (Fig. 2S). The growth trajectories of GFP-AtEB1-labelled microtubules appeared to first form a few antiparallel bundles (Fig. 2D,E, red arrows; see also Movie 1 in supplementary material) and, subsequently, other microtubules seemed to align to these structures to initiate the spindle (Fig. 2F,G). At these initial stages of spindle assembly, the GFP-AtEB1-labelled microtubule plus ends were distributed in the entire spindle area, which suggests massive microtubule growth in this area (Fig. 2F,G,T,U). Within the next 10 minutes, when the spindle acquired its characteristic shape, showing chromosomal congression (seen as negatively stained dark bodies at metaphase plate), GFP-AtEB1 comets gradually appeared largely at the spindle equator (Fig. 2H-J), indicating more microtubule growth events around the metaphase plate. The GFP-AtEB1 fluorescence intensity-profile along the spindle axis (Fig. 2K) clearly shows the initial concentration of microtubule growth around the NE and the gradual translocation of GFP-AtEB1 fluorescence intensity inside the nuclear area. Together, our results suggest that, during the process of spindle assembly, microtubules originated from the microtubule-cage around the NE invade the space around chromosomes and form a few bipolar bundles, which apparently define the major spindle axis. Subsequently, the spindle builds up involving many microtubule growth events within the preceding nuclear area.

Metaphase microtubules grow mostly towards but also away from chromosomes

During metaphase, we still observed massive microtubule growth events in the spindle (Fig. 2J,K). In order to understand the polarity and dynamics of microtubules within the

metaphase spindle, we analyzed the growth direction and the growth speed of GFP-AtEB1-stained microtubules in the metaphase spindle (Fig. 3; see also Movie 2 in supplementary material). For quantifying movements of polymerizing plus ends over time, kymographs were assembled (xt - or yt -plots) with lines drawn all along the spindle axis (yt -plots, Fig. 3C,I), or perpendicular to the spindle axis (xt -plot, Fig. 3A), from the time-lapse measurements (xyt). Visual inspection of movies and these constructed kymographs revealed that metaphase plant chromosomes (seen as a negative stain) maintained their positions without appreciable movements in x or y direction (Fig. 3A-D). Microtubule (plus end) growth is mainly noticeable along the spindle (y) axis and is bidirectional at both sides of the metaphase plate (Fig. 3C,I). A single yt -kymograph of a metaphase spindle constitutes numerous microtubule growth trajectories (seen as lines in the kymographs). Lines with a negative slope indicate growth from top to bottom, whereas lines with a positive slope represent growth from bottom to top. For the analysis we first concentrated on microtubule growth events along the spindle axis (yt) near the metaphase plate. For this, we discriminated growth events above and below chromosomes, for areas containing

chromosomes (Fig. 3A,B, left line; C,D,E-H) and areas lacking the chromosomes but containing overlapping microtubules (Fig. 3A,B, right line; I,J,K-N). For this discrimination, we used the negative stain of GFP-AtEB1 at the metaphase plate as a marker for chromosomal presence. Many overlapping microtubules originate at one side of the spindle, cross the metaphase plate and continue to grow at the opposite side in the direction of the spindle pole (see continuous lines crossing the metaphase plate in Fig. 3I). However, at the chromosomal area (Fig. 3C), only a few microtubules appear to grow across the metaphase plate. Careful inspection of Fig. 3C shows that the majority of microtubules (75%) in this area grow towards the chromosome (lines with negative slope in the top half of the kymograph Fig. 3C and lines with positive slope on the bottom half of the kymograph Fig. 3C) but, upon reaching the chromosome, further extension of their plus end labelling is lost, indicating an arrest of growth, or catastrophe. Also a small percentage (25%) of lines with opposite direction can be observed, starting their growth trajectory near the chromosome and growing away from them. The abrupt end of growth of some of the microtubules growing towards the chromosomes indicates that chromosomal presence induces catastrophes.

Since in the above/below focal planes we failed to see an increase in GFP-AtEB1 fluorescence near the chromosomes (not shown), it seems unlikely that the loss of fluorescence near the chromosomes is caused by a change of growth direction of the microtubules. In support another study has been demonstrated that upon changing their growth direction for more than 40 degrees, plant microtubules undergo an instant catastrophe (Dixit and Cyr, 2004). In addition, a few faint lines are seen that cross the chromosomal region. These faint lines most probably represent microtubule tracks of nearly out-of-focus overlapping microtubules not hindered by chromosomal presence.

To get an unbiased estimate of the polarity of microtubule growth close to

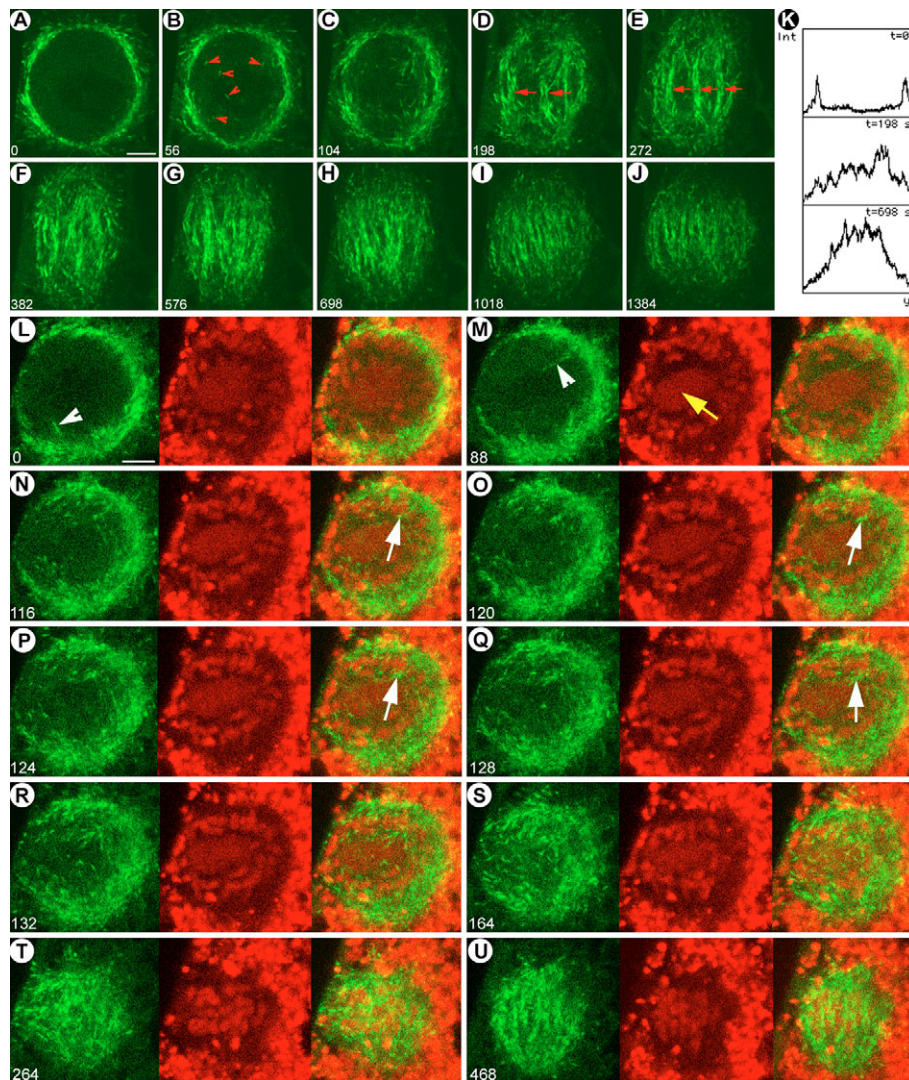


Fig. 2. Microtubule dynamics during spindle initiation. (A-J) Microtubule dynamics revealed by GFP-AtEB1 microtubule labelling during spindle assembly. Red arrowheads (B) show microtubule plus ends and red arrows (D,E) show microtubule bundles. (K) Fluorescence intensity profile of GFP-AtEB1 along the spindle axis (longitudinal axis extending through poles), corresponding to A,D and H. (L-U) Combined dynamics of microtubule (green) and chromosome (red) during spindle assembly. White arrows point to microtubule plus ends and the yellow arrow shows the nucleolus. Bar, 5 μ m; time is indicated in seconds.

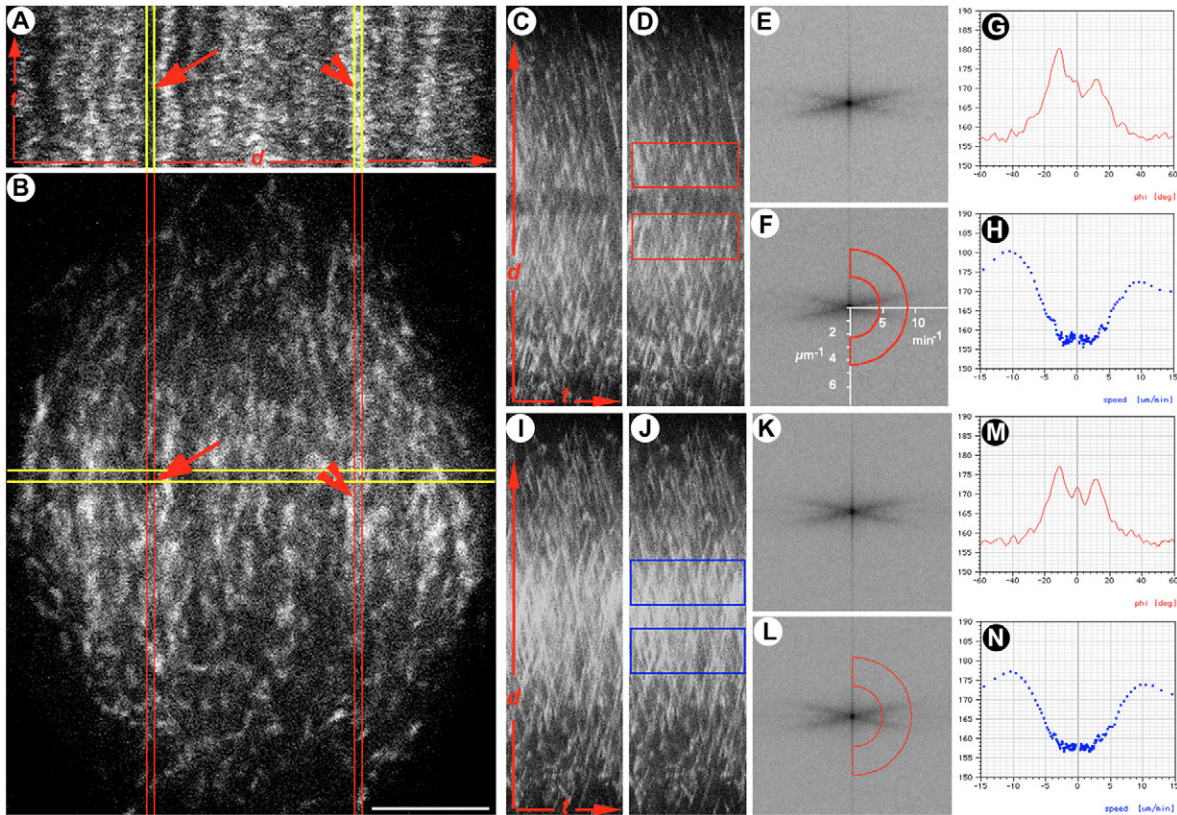


Fig. 3. Growth polarity and growth speed of spindle microtubules during metaphase. (A) ‘*xr*’ kymograph (horizontal line projection) of GFP-AtEB1-labelled spindle microtubules corresponding to the equatorial position in B (see corresponding arrows and arrowheads showing hardly any lateral movement of the areas containing chromosomes and those without chromosomes; yellow lines in A exactly match the areas shown by red lines in B, except that the yellow lines represent horizontal projection and the red lines vertical projection). (B) Metaphase spindle microtubules labelled with GFP-AtEB1. This is an initial image of a time-lapse series shown in Movie 2 from supplementary material. Panels C-H correspond to chromosomal areas and panels I-N correspond to overlapping microtubule areas without chromosomes near the equator. (C,D) ‘*yr*’ kymograph obtained from the left line drawn in B. (I,J) ‘*yr*’ kymograph obtained from the right line drawn in B. Rectangles in D and J indicate the areas taken for the Fourier analysis. The Fourier transformed images of the combined kymographs of all near chromosomal areas and of all overlapping microtubule areas without chromosomes in the entire spindle are given in E and K, respectively. All areas and individual kymographs are shown separately in supplementary material Fig. S2. The areas selected for obtaining the microtubule growth speeds from the Fourier images are shown in F and L. The specially developed image processing program Object-Image was used, which allows detector regions to be defined based on a local, polar co-ordinate system. A ring sector region of ± 90 degrees was marked (F,L), with clockwise angles as positive and the x -axis corresponding to zero degrees for averaging the pixels with the same angle and yielding an angular intensity profile (G). (G,M) Angular intensity distribution of Fourier graph (F) and (L). (H,N) Graph with reciprocal x -axis (from graph G and M) showing microtubule growth speed distribution in spindle areas. Bar, 7 μm .

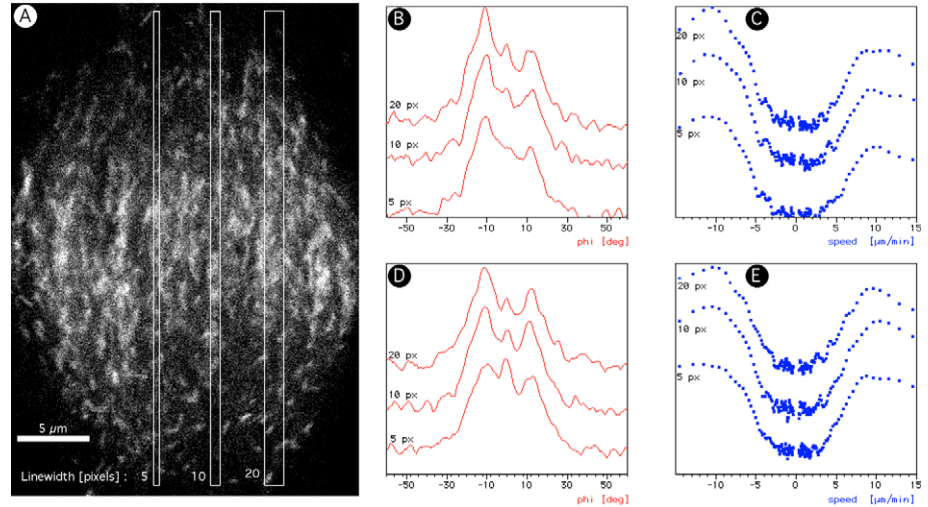
the metaphase plate in the areas with mainly overlapping microtubules (Fig. 3I) and areas near chromosomes (Fig. 3C), we analyzed the kymographs by a novel Fourier transform method. The concept of this Fourier approach is that images showing many parallel lines are transformed to an image with only one line rotated by 90 degrees. Hence, images showing many lines with two different slopes (i.e. our *yr*-kymographs) are transformed to a Fourier image with only two lines with 90 degrees tilted slopes. We reasoned that the intensity and slope of these two lines found in the Fourier image provides an unbiased overall estimate of both polarity distribution and speed of microtubule growth events.

First we evaluated how the thickness of the vertical line shown in Fig. 3B influences the Fourier analysis. Since the EB1 comets have a certain thickness in the measured time-lapse images, the line width in which we analyzed growth events should not be too big (reducing resolution for single

microtubule growth events) but also not too thin for reducing sensitivity to small x -directed microtubule-fluctuations. In Fig. 4, three analyses are shown for three line thicknesses. From the angular distribution plots and microtubule growth speed distribution plots (Fig. 4B,D and C,E, respectively), it is inferred that line thickness is not critical for our analysis. The line width of 0.7 μm (being slightly wider than a detected GFP-AtEB1) was found to be satisfactory.

Subsequently, we validated our Fourier analysis of kymographs by simulation. To this end, we generated images showing lines with one defined slope but random length and position in the image (Fig. 5A, left). As seen in the Fourier-transformed image (Fig. 5A, middle) this yields one line tilted 90 degrees. In the corresponding angular distribution plot (Fig. 5A, right), the highest intensity is found at exactly 30 degrees (being the input angle). However, the intensity was clearly distributed over a peak differing from a needle-like pattern (as

Fig. 4. Effect of line width on spindle kymograph analysis. Spindle kymograph analysis was performed as described in Fig. 3 and supplementary Fig. S2. To create a kymograph, a vertical rectangular region of interest (roi) in the x - y scan (A) was used, from which a vertical single pixel column was generated via the brightest point horizontal (x -directed) projection. The width of the roi was varied to investigate the effect of horizontal sampling range on the Fourier analysis. Three line widths were used; 5, 10 and 20 pixels corresponding to 0.35, 0.7 and 1.4 μm , respectively, as shown in A. Panels B and C correspond to the analysis of the near chromosomal areas, also shown in Fig. 3G and H, respectively; panels D and E correspond to the analysis of overlapping microtubule areas, also shown in Fig. 3M and N, respectively.



was used for input). This most probably is caused by line thickness, several lines touching each other adjacently, and pixel superposition effects in the input image. Next, we simulated a symmetric bipolar situation where lines with an angle of 20 and -20 degrees were simulated at random positions (Fig. 5B, left). Now the corresponding Fourier image indeed shows two lines of equal intensity, both tilted 90 degrees to the original image (Fig. 5B, middle). The angular distribution plot (Fig. 5B, right) now is clearly symmetric, and the peak positions again exactly match the input values. Also we simulated an asymmetric bipolar situation (Fig. 5C). Here differences in intensity are seen between the two lines in the Fourier image (Fig. 5C, middle) causing an asymmetric angular distribution plot (Fig. 5C, right). Again the peak positions in this distribution plot are correct indicators of the slope of the lines in the simulated image Fig. 5C. However, the peak heights seem only qualitatively related to the input population sizes. In Fig. 5D, we analyzed the situation of a single polarity but with a broadly distributed slope. In the corresponding Fourier image (Fig. 5D, middle), clearly a single but radially more diffuse line can be discerned. The top of the peak in the angular distribution plot appeared flat (Fig. 5D, right) and again matched the input parameters. We also systematically varied the slope of lines in the simulated kymographs. In the simulation shown in Fig. 5E, an asymmetric bipolar distribution was simulated (similar to Fig. 5C). But now the slope of the minor population of lines (10%) was varied between 10 and 70 degrees. For each distribution, a Fourier transform and an angular distribution plot (Fig. 5C, middle and right) was generated and the minor peak position (in degrees) was determined. As can be inferred from the excellent correlation between input angle and measured peak positions, the Fourier method performs very well in identifying contributions of minor populations of growth events regardless of their speed. Also the heterogeneity of microtubule growth speeds was simulated. Narrow distribution (one predominant speed) and very broadly evenly distributed speeds (up to 30 degrees slope difference in the kymograph plots) were simulated and the width of the angular speed distribution was plotted against the input heterogeneity. It can be seen that input and output are positively correlated; indicating that small and large heterogeneity in microtubule growth speed distributions

can be identified with our Fourier analysis. However, our Fourier analysis particularly at more uniformly distributed input values overestimates the heterogeneity. Together this demonstrates that the Fourier method (1) gives a very accurate estimate of growth speed, (2) is able to discriminate unidirectional growth from the bidirectional growth, and (3) gives a qualitative view on polarity distribution within a complex and crowded structures such as the spindle.

We performed the Fourier analysis not on one representative kymograph (shown in Fig. 3C,I) but on many *yt*-kymographs obtained from the entire spindle area (supplementary material Fig. S2). First, at intervals of 0.7 μm along the x -axis, separate kymographs were made. Then, based on the negatively stained chromosomes we marked the near chromosomal and overlapping microtubule areas by drawing rectangles above and below the equator (representative examples are shown in Fig. 3D,J). Afterwards we pasted all rectangular regions one by one as a montage and flipped the direction of the rectangles obtained from the areas below the equator to match the direction of the rectangles obtained from the areas above the equator. The two montages obtained were subjected to Fourier transformation. The resulting whole-spindle kymograph Fourier-transforms are shown in Fig. 3E (for near chromosome microtubule growths) and in Fig. 3K (for areas containing overlapping microtubules but lacking chromosomes). These Fourier-transformed images indeed showed two lines tilted 90 degrees with respect to the lines observed in the kymographs. We quantitatively analyzed the intensity and slope of the lines in the Fourier-images to obtain the average growth speed and polarity distribution of microtubule growth. As shown in Fig. 3E-H,K,N, the distribution of microtubular growth rate was directly obtained from the Fourier graphs. From the maxima of the growth-speed distribution plots in Fig. 3H,N, it is easily inferred that, regardless of direction, microtubule growth among all the regions of the spindle occurs at 10 $\mu\text{m}/\text{minute}$. To confirm the microtubule growth rate obtained from Fourier analysis, we manually tracked individual microtubule plus ends and measured their growth rates. Similarly to the Fourier analysis, the manual tracking revealed that microtubules in metaphase plant spindle grow at $10.1 \pm 0.6 \mu\text{m}/\text{minute}$ ($n=42$). This microtubule growth rate compares well with that observed in *Xenopus* egg extracts spindles (Tirnauer et al., 2004). Since

the growth distribution plot in Fig. 3H has a lower maximum for positive slopes than for negative slopes, we inferred that there were more microtubules growing towards chromosomes than microtubules growing away from chromosomes (Fig. 3E). In the case of overlapping microtubule in areas devoid of chromosomes near the equator, the difference between the opposite polarities was minute (Fig. 3K,N). Therefore, the Fourier-based analysis of microtubule polarity in metaphase spindles clearly shows bipolar overlapping microtubule bundles crossing the metaphase plate and growing at $10 \mu\text{m}/\text{minute}$ and shows that in the vicinity of chromosomes more microtubules grow towards the chromosome than away from them.

To compare the extent of microtubule bipolarity and microtubule growth speed in regions close to the equator and close to the poles of plant spindles we vertically divided the spindle kymographs into four consecutive parts along the spindle (y) axis (Fig. 6A,B) and performed a similar Fourier-transform analysis (Fig. 6C). As can be inferred from Fig. 6C,D, microtubule growth is more unidirectional at the spindle pole and more bidirectional at the equator. From the analysis shown in Fig. 6, we concluded that most of the microtubules growing from opposite poles overlap mainly at the equator with very few of them spanning the whole pole-to-pole distance. In the case of microtubules originating near the poles and overlapping at the equator, the intensity of the equator should remain double that of the poles. In reality, the intensity of GFP-AtEB1-labelled microtubule growth was much stronger at the equator (see also bottom profile in Fig. 2K and top profile in Fig. 7J). This suggests increased dynamic instability (giving rise to more growth events of a single microtubule) and/or new microtubule initiations around the equator. By comparing the intensity profile plots across the metaphase spindle axis of GFP-MAP4, labelling entire microtubules (supplementary material Fig. S3), with that of GFP-AtEB1, marking MT-growth events (Fig. 2K and Fig. 7J), we see that the concentration of GFP-AtEB1 is more pronounced at the equator than that of GFP-MAP4. This difference suggests that near the equator, dynamic instability is upregulated. In addition, we see that the GFP-MAP4 label shows highest concentration near the equator, although its intensity profile is more flat. Hence, more microtubules (mass levels) are present near the equator than at the poles. Together, these data suggest that, in addition to microtubule dynamic instability, microtubule initiation is upregulated near the equator. As a spindle bears high microtubule density, observation of individual microtubule catastrophe and rescue within such a crowded structure is technically not yet possible. Interestingly, a previous *in vitro* study in which microtubule depolymerisation was induced by severing *Xenopus* spindles with a microneedle revealed fewer rescue and regrowth events (Tirmauer et al., 2004). Interestingly, microtubule growth rates obtained from Fourier transformations for all four quarters along the spindle axis (Fig. 6D) remained the same ($10 \mu\text{m}/\text{minute}$). This indicates that

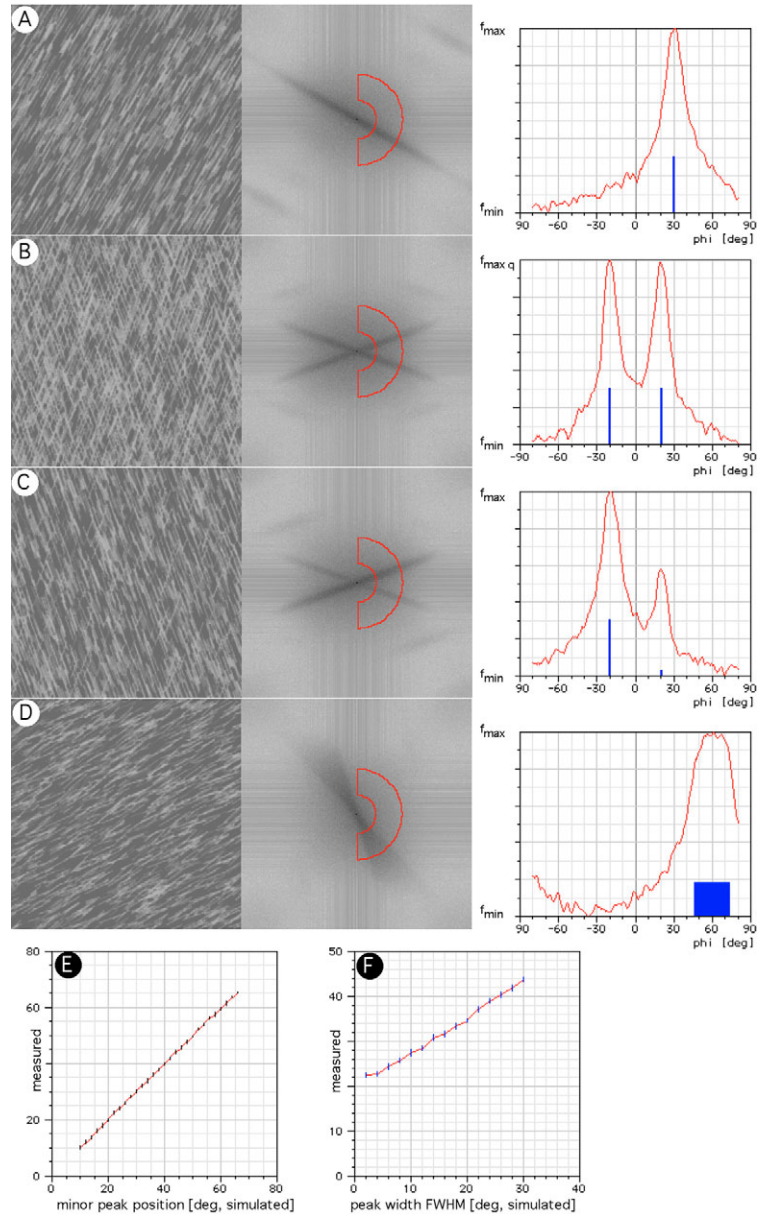


Fig. 5. Validation of Fourier-based kymograph analysis by simulation. (A-D) Left, Simulated kymograph; middle, power spectrum of Fourier transform and ring sector; right, angular distribution plots (corresponding to speeds) in the kymograph (blue, input; red, output as measured inside the ring sector). (A) Simulation of unidirectional growth with narrow distribution of growth speeds. (B) Simulation of bidirectional growth with symmetrical distribution of growth speeds. (C) Simulation of bidirectional growth with asymmetrical distribution of growth speeds; input frequencies differ by a factor of 10. (D) Simulation of unidirectional growth with broad distribution of growth speeds. (E) Measured versus theoretical minor peak position in simulation C, where the major peak remained fixed and the minor peak varied from 10 to 70 degrees. Vertical bars represent standard deviation of 10 independent simulations. (F) Theoretical peak width of measured velocities (FWHM) in simulation D; input peak width varied from 2 to 30 degrees. Vertical bars represent standard deviation of 10 independent simulations.

chromosomal vicinity apparently modulates parameters other than microtubular growth rate in regulating microtubular dynamic instability and/or initiation.

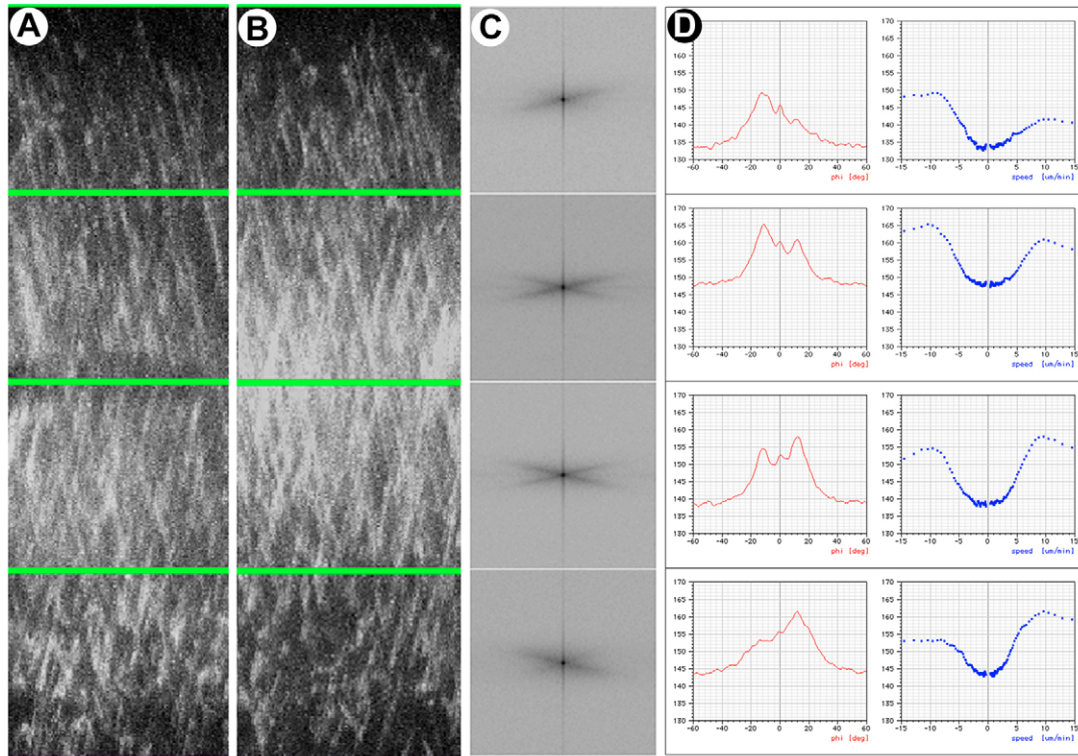


Fig. 6. Microtubule polarity and growth speed along the spindle-axis. Kymograph obtained from a line drawn over a chromosomal area (A) and overlapping microtubule area without chromosome (B) displaying growth polarity of GFP-AtEB1-labelled spindle microtubules. Fourier graphs in C are obtained from four parts of the combined kymograph representing the entire spindle area, which is assembled from various kymographs obtained by drawing subsequent lines on whole spindle area. (D) Angular intensity distribution and growth speed distribution of the Fourier graphs from C.

Spindle equator-to-pole movement of chromatids displays biphasic kinetics

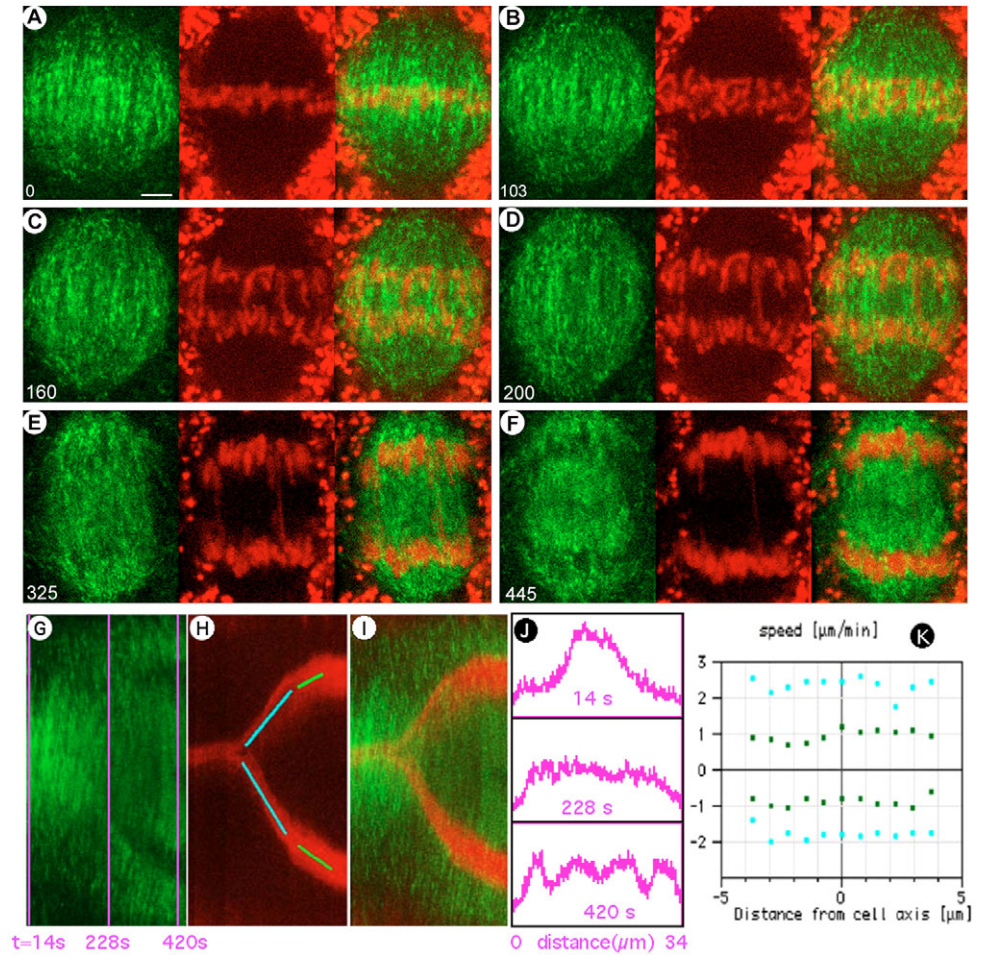
To reveal the combined dynamics of microtubules and chromosomes at the onset of anaphase we performed dual visualization of GFP-AtEB1-labelled microtubule plus ends and SYTO82-labelled chromosomes (Fig. 7A-F; see also Movie 3 in supplementary material). The speed of chromosome motion was measured from the assembled kymographs of the entire spindle of which one representative kymograph is shown in Fig. 7G-I. Interestingly, for all the 22 chromosomes, two distinct phases of chromosome motion involving different translocation speeds were observed (Fig. 7K) as shown by the two coloured line pairs drawn on the chromosomal path (Fig. 7H). During the first phase, chromosomes moved faster, at $2.1 \pm 0.3 \mu\text{m}/\text{minute}$ ($n=34$), while in the subsequent phase, when they were close to the poles, their movement was reduced to $0.9 \pm 0.1 \mu\text{m}/\text{minute}$ ($n=34$). Similarly to metaphase, GFP-AtEB1-labelled microtubules displayed bidirectional growths near the chromosomes until the onset of chromosomal separation (Fig. 7G). Interestingly, at the onset of chromatid separation, GFP-AtEB1 fluorescence, in chromosomal vicinity was reduced (as inferred from the kymograph in Fig. 7G and the pixel intensity profiles in Fig. 7J). Fig. 7C,D also displays less intense GFP-AtEB1 labelling between separating chromatids in comparison with its signal at the poles or in comparison to adjacent areas with overlapping microtubules (devoid of chromosomes). As GFP-AtEB1 does not label shrinking microtubules, reduction in GFP-AtEB1 intensity can result from microtubule

depolymerization around the chromosomes at the onset of their separation. Concomitantly with the chromosomes beginning the second (slow) phase of their poleward movement, many microtubules initiated their growth (as evidenced by enhanced GFP-AtEB1 fluorescence in Fig. 7F,G and from the pixel intensity profiles in Fig. 7J) towards the equator where the phragmoplast (a cytokinetic plant cell-specific structure) begins to form.

Microtubules in the plant spindle exhibit flux with its speed matching the pace of chromatid separation

To investigate whether microtubules in plant spindles display poleward flux, we created photobleached marks on GFP- α tubulin 6 (GFP-TUA6)-labelled metaphase microtubules and followed their dynamics. In contrast to GFP-AtEB1 and GFP-MAP4, GFP-TUA6 stably incorporates into spindle-microtubules along their entire length, enabling monitoring of flux by observing the movement of photobleached marks. Line bleaching was performed equidistant from the spindle equator during metaphase and during the metaphase-anaphase transition. Strikingly, at metaphase the bleached areas moved towards the spindle poles (Fig. 8A-D; see also Movie 4 in supplementary material) with a velocity of $2 \pm 0.2 \mu\text{m}/\text{minute}$ ($n=10$). The corresponding fluorescence intensity profiles projected sequentially on a time axis clearly showed translocation of the photobleached area towards the spindle poles (Fig. 8I,J). To our knowledge, this is the first time that microtubule-flux has been shown in acentrosomal plant spindles.

Fig. 7. Dynamics of chromosome movements during anaphase. Green: GFP-AtEB1, and Red: SYTO82-DNA staining (chromosomes inside and mitochondria outside the spindle area). (A-F) Combined microtubular and chromosome dynamics at anaphase (Movie 3 in supplementary material). (G) Kymograph obtained by drawing a line on one of the chromosomes from the anaphase spindle. (H) Phases of poleward motion of chromosome during anaphase. (I) Merged kymograph showing both microtubule growth and chromosome motion. (J) Fluorescence intensity profile of GFP-AtEB1 along the spindle axis (pole to pole axis) during anaphase obtained from lines drawn at three time points (shown in G). The x axis represents pole to pole distance in μm and y axis shows fluorescence intensity in an arbitrary scale. Note that all three panels are at the same fluorescence intensity scale. (K) Speed of individual chromosome motion (represented by each dot) along with its respective position in the spindle. 0 represents a pole-to-pole axis passing through the centre of the spindle equator and left and right sides depict the distance in relation to this spindle axis. The dots show the relative positions of various chromosomes from the spindle axis. Blue dots show the speed of chromosomes during the first (fast) phase of anaphase, whereas green dots show the speed of chromosomes during the second (slow) phase of anaphase. The y axis represents the speed ($\mu\text{m}/\text{minute}$) of individual chromosomes. Bar, $5 \mu\text{m}$; time is indicated in seconds.



In order to assess the rate of flux during the metaphase to anaphase transition, we performed the photobleaching experiments exactly at a time when chromosomes initiated their polar movements (Fig. 8E-H). At the metaphase-anaphase transition, the velocity of microtubule-translocation, as measured from the movement of the photobleached area, remained $2 \pm 0.1 \mu\text{m}/\text{minute}$ ($n=10$) (similar to velocity at metaphase) (Fig. 8E-H; see also Movie 5 in supplementary material). Remarkably, the speed of microtubule flux (Fig. 8E-H,K) was the same as the speed of chromatid separation (Fig. 7K) suggesting a link between microtubule flux and chromatid separation.

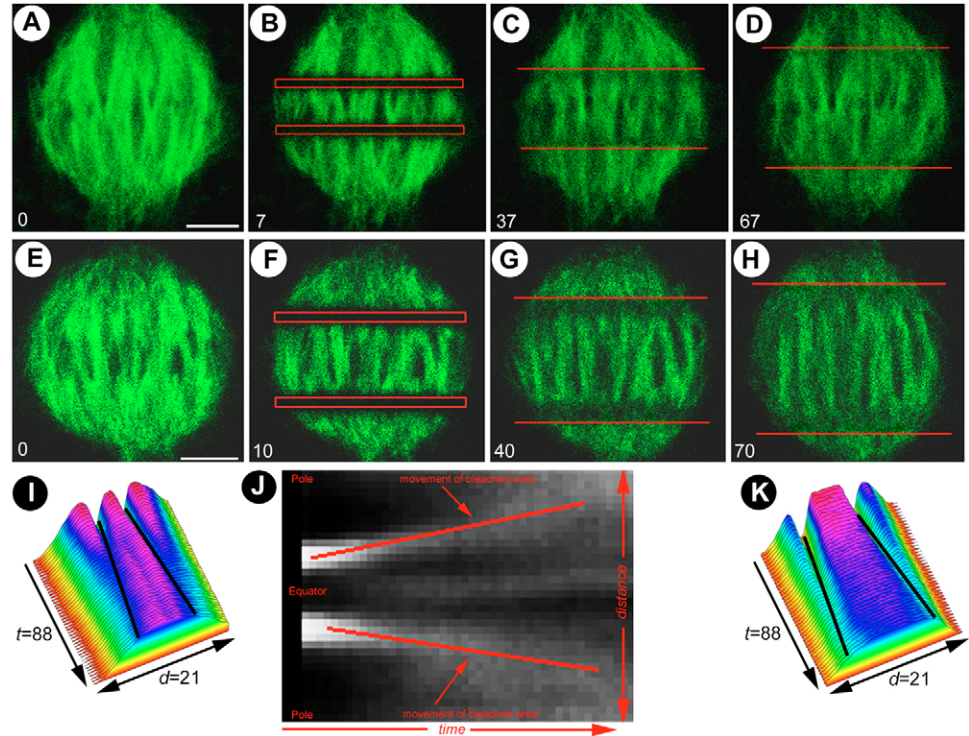
Discussion

Our results provide detailed mechanistic insight for the assembly and functioning of acentrosomal spindles formed in plant cells as they reveal (1) the contribution of NE-microtubules for spindle assembly, (2) the polarity and growth speed of microtubule growths among the entire metaphase spindle and (3) the occurrence of tubulin flux both during metaphase and anaphase with matching of the rate of tubulin flux to the speed of chromatid separation.

What is the importance of microtubule accumulation on the NE and their subsequent penetrations inside the NE?

At the onset of mitosis, in addition to forming the cortical PPB containing microtubules with bidirectional growth polarity (Dhonukshe and Gadella, Jr, 2003), microtubules gradually appear on the NE, radiating in all directions. Some of the microtubules that are radiating from the NE form bipolar bundles with microtubules growing from the cell cortex towards the NE, and these bundles position the nucleus at the cell centre as described before (Dhonukshe et al., 2005). Rearrangement of the microtubule meshwork radiating from the nuclear surface and the formation of a dense microtubular cage around the nucleus has been reported before for the lower plant *Hemanthus* endosperm (Smirnova and Bajer, 1998) and for mammalian cells (Piehl and Cassimeris, 2003). Previously, ultrastructural observations of *Hemanthus* endosperm showed that around the time of NE breakdown it becomes sharply undulated with the formation of ripples at the poles (De Mey et al., 1982; Smirnova and Bajer, 1998). More recently, a detailed live cell microscopy of mammalian cells showed the role of microtubules in the mechanical rupture of the NE during prophase (Beaudouin et al., 2002). Another study performed

Fig. 8. Occurrence of microtubule flux in plant spindles. (A–D) Movement of photobleached lines marked on spindle microtubules during metaphase (Movie 4 in supplementary material). (E–H) Movement of photobleached lines marked on spindle microtubules during anaphase (Movie 5 in supplementary material). Panels I and K represent fluorescence intensity profiles projected sequentially on time axes showing translocation of the photobleached area corresponding to images A–D and E–H, respectively. t represents time in seconds and d indicates distance in μm . J represents a difference kymograph of I, showing the gain of fluorescence along the spindle axis immediately after photobleaching, clearly demonstrating microtubule translocation towards the spindle poles. Bar, 5 μm ; time is indicated in seconds



on BY-2 cells by use of GFP-MAP4 and a NE lamina marker has shown that the NE breakdown precedes PPB disappearance (Dixit and Cyr, 2002), similarly to what we (indirectly) observed using FM4-64. Together these findings suggest a mechanism by which microtubules in premitotic plant cells first invade the nucleus by creating initial punctures, followed by NE breakdown similar to that in premitotic mammalian cells. Yet it remains to be established whether microtubular punctures are instrumental in causing NE rupture in plants, or that a gradual NE breakdown (by a process independent of microtubule dynamics) results in increasing the permeability of the NE, allowing first microtubules to enter the nuclear area and subsequently larger structures such as endosomes.

How does microtubule growth polarity in plant spindles look in comparison with other species?

Compared with acentrosomal (plant) spindles, centrosome-originated spindles in other species display less dense microtubule overlap at the equator and substantial chromosomal oscillations (Rieder and Salmon, 1998). In contrast, typical acentrosomal spindles from oocytes and lower plant *Hemanthus* endosperm (Bajer and Mole-Bajer, 1971; Rieder and Salmon, 1994; Khodjakov et al., 1996) do not display chromosomal oscillations and have more dense overlapping microtubules (Desai et al., 1998; Maddox et al., 2002). The density of overlapping microtubules at the equatorial region is more than twofold higher compared with that at the spindle poles (see the GFP-MAP4 intensity profile in supplementary material Fig. S3) (Desai et al., 1998; Maddox et al., 2002). According to the self assembly mechanism, the cytoplasmic area of about 4 to 8 μm remaining in the chromosomal vicinity creates a state that induces microtubule assembly (Carazo-Salas et al., 1999; Karsenti and Vernos, 2001; Niethammer et al., 2004), which results in the formation

of dense overlap-class spindles. These previous observations have been strongly supported by a recent excellent analysis (Caudron et al., 2005) showing that a GTP-bound gradient signal orchestrates the mitotic spindle assembly in *Xenopus* egg extracts.

Previously drug treatments in plant cells (Falconer et al., 1988; Binarova et al., 1998) and other observations in diverse species (Karsenti and Vernos, 2001) have suggested microtubule-initiations near chromosomes. For instance, it has been shown for plant cells that a universal MTOC component γ -tubulin remains associated with the centromere-kinetochore region starting from the prophase until the late anaphase (Binarova et al., 1998). During spindle assembly in some lower plants, γ -tubulin extends from the polar regions to the metaphase plate, which suggests that microtubule nucleation sites translocate towards the chromosomes (Brown et al., 2004). In mammalian cells also, microtubules are nucleated at chromosomes *in vitro* and *in vivo* (Telzer et al., 1975; Pepper and Brinkley, 1979; Bergen et al., 1980; Mitchison and Kirschner, 1985). Recently, chromosome-originated kinetochore fibre-formation has been observed *in vivo* in centrosomal *Drosophila* S2 cells both during prometaphase and metaphase, suggesting the persistent capacity of kinetochores to nucleate microtubules *in vivo* (Maiato et al., 2004). Therefore our results showing partial bipolarity of microtubule growth events close to the chromosomes does not exclude the possibility of microtubule emergence near plant chromosomes. Mitchison discusses that, in plant spindles, kinetochore microtubules account for approximately 5% of the total spindle microtubules, which is similar to what has been observed in *Xenopus* extract spindles (Mitchison, 2005). In addition, *Xenopus* extract spindles assemble to normal morphology in the absence of kinetochores (Karsenti and Vernos, 2001), which indicates their dispensability. This

further suggests that most of the microtubules in the vicinity of chromosomes in *Xenopus* extract (and plant spindles) are non-kinetochore microtubules, some of which interact laterally with the centromere and co-bundle with kinetochore microtubules (Jensen, 1982; McDonald et al., 1992). Recently, Maiato et al. have also shown that, at initial time points, kinetochore fibres are oriented away from chromosomes and, as they grow, their non-growing (minus) ends are captured by centrosome-originated astral microtubules and transported poleward through a dynein-dependent mechanism so that they can be oriented towards chromosomes (Maiato et al., 2004). Dynein RNAi impairs kinetochore fibre orientation. However, based on the available genome sequences, some higher plants, especially the dicots (*Arabidopsis*, Tobacco, etc.), lack dynein, and therefore it is unclear whether similar transport and orientation will occur in higher plants. Nevertheless, we hypothesize that some of these near-chromosome-localized shorter microtubules physically interact with pole-originated microtubules, either by microtubular crosslinking factors or by motor proteins, allowing the interactions necessary for microtubule sliding, which can contribute to force generation on chromosomes (Mitchison, 2005). In this respect, we mention a recent *in vivo* analysis of the microtubule crosslinking factor MAP65a from *Arabidopsis* (Chang et al., 2005; Mao et al., 2005); however, its absence on metaphase microtubules would suggest the existence of an as yet unidentified crosslinking factor acting at metaphase.

How does anaphase chromosome movement look in plant spindles?

Our results show that the spindle equator-to-pole movement of chromatids displays biphasic kinetics: faster at the initiation and slower at the end. Most likely the first faster phase seems to be the sum of anaphase A and anaphase B, whereas the second slower phase resembles anaphase B. Without the differentiation of fast and slow phase, similar chromosome separation speeds were measured previously in plant cells (Barber, 1939; Hepler and Palevitz, 1986; Ryan, 1983) and in *Xenopus* egg extracts (Desai et al., 1998), whereas higher separation speeds have been observed in *Haemaphysalis* endosperm cells (Khodjakov et al., 1996) and in *Drosophila* embryos (Maddox et al., 2002), which suggests cell-type-specific differences.

What are the implications of flux in plant spindles?

Our photobleach mark analysis shows that spindle microtubules in plant cells flux. As the flux rate and chromosome separation speed match, we propose microtubule flux as the prime process driving the chromosome separation in acentrosomal plant cells. Previous observations from *Hemanthus* endosperm cells (Khodjakov et al., 1996) support our view. In *Hemanthus* endosperm a severed arm of a metaphase chromosome is found to be transported poleward (instead of ejecting away from the nearest pole by a polar wind) with a velocity similar to that exhibited by chromosomal movements during anaphase (Khodjakov et al., 1996). In addition, microtubule flux in metaphase plant spindles correlates with the non-oscillatory motion of the congressed chromosomes since spindles with fast flux rates do not display chromosomal oscillations (Desai et al., 1998). Minus end-disassembly is the dominant mechanism in mammalian centrosomal spindles displaying the flux (Waters et al., 1996),

whereas acentrosomal spindles assembled in *Xenopus* egg extracts seem to use mainly the sliding force (Miyamoto et al., 2004; Shirasu-Hiza et al., 2004) in addition to the minus end-disassembly. To better understand the force driving flux in plant spindles, it will be necessary to investigate the contribution of microtubule depolymerization at the poles (Rogers et al., 2004; Rogers et al., 2005) and microtubule sliding (Miyamoto et al., 2004).

In conclusion, our analysis of microtubules in acentrosomal plant spindles reveals striking similarities of spindle biogenesis process among plants and other systems where continuous bipolar microtubule growth and tubulin flux assembles and maintains the spindle structure. The novel Fourier-based analysis of kymograph data gives unbiased quantitative assessment of microtubule growth dynamics among the entire spindle. This for the first time provides detailed mechanistic insight for spindle formation and functioning in plant cells. As the components regulating flux seem to be conserved in plants (Reddy and Day, 2001) it will be an important future task to sort out which of these components regulate microtubule flux in plant spindles in order to gain a complete molecular understanding of the secrets of acentrosomal spindle dynamics in walled plant cells.

Materials and Methods

Plant material and growth conditions

Tobacco BY-2 cells were cultured and transformed as reported previously (Dhonukshe and Gadella, Jr, 2003).

Construction of reporter genes

Construction of GFP-*Arabidopsis* EB1 (GFP-AtEB1) (Mathur et al., 2003), GFP- α tubulin 6 (GFP-TUA6) (Ueda et al., 1999) and GFP-MAP4 (Dhonukshe and Gadella, Jr, 2003) has been described previously.

Fluorescent dyes

SYTO82 and FM4-64 (Molecular Probes) were used at 1 μ M final concentration.

Live cell analysis and data processing

For live cell analysis, the Zeiss CLSM510 system implemented on an inverted (Axiovert 100) microscope was used. The microscopy system, sample preparation, single wavelength scanning and movie generation was described before (Dhonukshe and Gadella, Jr, 2003). On the confocal microscope, the cylindrical plant cells were mounted horizontally and scanned at constant z position, resulting in mid-cell cross-sections parallel to the cell axis. For time-lapse analysis, images were obtained at 1-10 seconds time intervals. Post-acquisition image processing was performed with the public domain program Object-Image version 2.12 (by N. Vischer, <http://simon.bio.uva.nl/object-image.html>, based on NIH Image by W. Rasband). To study the movement of microtubules, kymographs (yz images) were used. To create a kymograph, we defined a vertical rectangular region of interest (width 0.7 μ m at full height) in the x - y scan at a certain x position, projected it into a single pixel column via the brightest point projection, and accumulated the columns along the horizontal time axis (e.g. Fig. 3C). Transforming the kymograph into a Fourier domain results in an X-shaped pattern; the rising and falling arm correspond to movements in opposite directions (in this case to and away from the equator, respectively). The object image program allows defining detector regions based on a local co-ordinate system; here a polar co-ordinate system in combination with a ring sector region of ± 90 degrees with respect to the x axis was used, where clockwise angles are positive. Fig. 3G shows the transversal intensity profile of the detector region, while Fig. 3H shows the same graph with reciprocal x -axis scaled in speed. The peaks in the graphs correspond to the most frequent speeds. Dual colour imaging of SYTO and GFP was performed using dual excitation/emission scanning in multitracking mode. We used excitation/emission combinations of 488 nm/BP 505-530 for GFP and 543 nm/LP560 for SYTO in combination with the HFT 488/543 primary and NFT545 secondary dichroic splitters. All filters were from Zeiss.

Photobleaching analysis

Photobleaching experiments were performed on mitotic metaphase or anaphase cells, using 100% laser power of 488 nm laser line in 6 seconds to obtain complete photobleaching of the marked areas. Five images at 2% laser power were taken before photobleaching. After photobleaching, images were acquired at ~ 2 second

time intervals, again using 2% of 488 laser line. The same microscope settings were used for multiple spindles analysed at metaphase and anaphase. Post-acquisition image processing to obtain the fluorescence intensity profiles was performed with the public domain program Object-Image version 2.12.

We thank Jaideep Mathur (University of Guelph, Canada) for the GFP-AtEB1 construct and Takashi Hashimoto (Nara Institute of Science and Technology, Japan) for the GFP-TUA6 construct. P.D. and T.W.J.G. were supported by the Netherlands Organization for Scientific Research (NWO FOM-ALW 805.47.012). T.W.J.G. was supported by NWO van der Leeuw 835.25.004 and by the EU-integrated project on Molecular Imaging LSHG-CT-2003-503259.

References

- Bajer, A. and Mole-Bajer, J. (1971). Architecture and function of the mitotic spindle. *Adv. Cell. Mol. Biol.* **1**, 213-266.
- Barber, H. N. (1939). The rate of movement of chromosomes on the spindle. *Chromosoma* **1**, 33-50.
- Beaudouin, J., Gerlich, D., Daigle, N., Eils, R. and Ellenberg, J. (2002). Nuclear envelope breakdown proceeds by microtubule-induced tearing of the lamina. *Cell* **108**, 83-96.
- Bergen, L. G., Kuriyama, R. and Borisy, G. G. (1980). Polarity of microtubules nucleated by centrosomes and chromosomes of Chinese hamster ovary cells in vitro. *J. Cell Biol.* **84**, 151-159.
- Binarova, P., Hause, B., Dolezel, J. and Draber, P. (1998). Association of gamma-tubulin with kinetochore/centromeric region of plant chromosomes. *Plant J.* **14**, 751-757.
- Bisgrove, S. R., Hable, W. E. and Kropf, D. L. (2004). +TIPs and microtubule regulation. The beginning of the plus end in plants. *Plant Physiol.* **136**, 3855-3863.
- Bonaccorsi, S., Giansanti, M. G. and Gatti, M. (1998). Spindle self-organization and cytokinesis during male meiosis in asterless mutants of *Drosophila melanogaster*. *J. Cell Biol.* **142**, 751-761.
- Brown, R. C., Lemmon, B. E. and Horio, T. (2004). Gamma-tubulin localization changes from discrete polar organizers to anastral spindles and phragmoplasts in mitosis of *Marchantia polymorpha* L. *Protoplasma* **224**, 187-193.
- Carazo-Salas, R. E. and Karsenti, E. (2003). Long-range communication between chromatin and microtubules in *Xenopus* egg extracts. *Curr. Biol.* **13**, 1728-1733.
- Carazo-Salas, R. E., Guarguaglini, G., Gruss, O. J., Segref, A., Karsenti, E. and Mattaj, J. W. (1999). Generation of GTP-bound Ran by RCC1 is required for chromatin-induced mitotic spindle formation. *Nature* **400**, 178-181.
- Caudron, M., Bunt, G., Bastieans, P. and Karsenti, E. (2005). Spatial coordination of spindle assembly by chromosome-mediated signalling gradients. *Science* **309**, 1373-1376.
- Chan, J., Calder, G. M., Doonan, J. H. and Lloyd, C. W. (2003). EB1 reveals mobile microtubule nucleation sites in *Arabidopsis*. *Nat. Cell Biol.* **5**, 967-971.
- Chan, J., Calder, G., Fox, S. and Lloyd, C. (2005). Localization of the microtubule end binding protein EB1 reveals alternative pathways of spindle development in *Arabidopsis* suspension cells. *Plant Cell* **17**, 1737-1748.
- Chang, H. Y., Smertenko, A. P., Igarashi, H., Dixon, D. P. and Hussey, P. J. (2005). Dynamic interaction of NtMAP65-1a with microtubules in vivo. *J. Cell Sci.* **118**, 3195-3201.
- De Mey, J., Lambert, A. M., Bajer, A. S., Moeremans, M. and De Brabander, M. (1982). Visualization of microtubules in interphase and mitotic plant cells of *Haemanthus* endosperm with the immuno-gold staining method. *Proc. Natl. Acad. Sci. USA* **79**, 1898-1902.
- Desai, A., Maddox, P. S., Mitchison, T. J. and Salmon, E. D. (1998). Anaphase A chromosome movement and poleward spindle microtubule flux occur at similar rates in *Xenopus* extract spindles. *J. Cell Biol.* **141**, 703-713.
- Dhonukshe, P. and Gadella, T. W., Jr (2003). Alteration of microtubule dynamic instability during preprophase band formation revealed by yellow fluorescent protein-CLIP170 microtubule plus-end labeling. *Plant Cell* **15**, 597-611.
- Dhonukshe, P., Mathur, J., Hulskamp, M. and Gadella, T., Jr (2005). Microtubule plus-ends reveal essential links between intracellular polarization and localized modulation of endocytosis during division-plane establishment in plant cells. *BMC Biol.* **3**, 11.
- Dhonukshe, P., Baluska, F., Schlicht, M., Hlavacka, A., Samaj, J., Friml, J. and Gadella, T. W., Jr (2006). Endocytosis of cell surface material mediates cell plate formation during plant cytokinesis. *Dev. Cell* **10**, 137-150.
- Dixit, R. and Cyr, R. J. (2002). Spatio-temporal relationship between nuclear-envelope breakdown and preprophase band disappearance in cultured tobacco cells. *Protoplasma* **219**, 116-121.
- Dixit, R. and Cyr, R. (2004). Encounters between dynamic cortical microtubules promote ordering of the cortical array through angle-dependent modifications of microtubule behaviour. *Plant Cell* **16**, 3274-3284.
- Emans, N., Zimmermann, S. and Fischer, R. (2002). Uptake of a fluorescent marker in plant cells is sensitive to brefeldin A and wortmannin. *Plant Cell* **14**, 71-86.
- Falconer, M. M., Donaldson, G. and Seagull, R. W. (1988). MTOCs in higher plant cells: an immunofluorescent study of microtubule assembly sites following depolemerization by APM. *Protoplasma* **144**, 46-55.
- Geelen, D. N. and Inze, D. G. (2001). A bright future for the bright yellow-2 cell culture. *Plant Physiol.* **127**, 1375-1379.
- Heald, R., Tournebise, R., Blank, T., Sandaltzopoulos, R., Becker, P., Hyman, A. and Karsenti, E. (1996). Self-organization of microtubules into bipolar spindles around artificial chromosomes in *Xenopus* egg extracts. *Nature* **382**, 420-425.
- Hepler, P. K. and Palevitz, B. A. (1986). Metabolic inhibitors block anaphase A in vivo. *J. Cell Biol.* **102**, 1995-2005.
- Jensen, C. G. (1982). Dynamics of spindle microtubule organization: kinetochore fiber microtubules of plant endosperm. *J. Cell Biol.* **92**, 540-558.
- Karsenti, E. and Vernos, I. (2001). The mitotic spindle: a self-made machine. *Science* **294**, 543-547.
- Khodjakov, A., Cole, R. W., Bajer, A. S. and Rieder, C. L. (1996). The force for poleward chromosome motion in *Haemanthus* cells acts along the length of the chromosome during metaphase but only at the kinetochore during anaphase. *J. Cell Biol.* **132**, 1093-1104.
- Khodjakov, A., Cole, R. W., Oakley, B. R. and Rieder, C. L. (2000). Centrosome-independent mitotic spindle formation in vertebrates. *Curr. Biol.* **10**, 59-67.
- Kirschner, M. and Mitchison, T. (1986). Beyond self-assembly: from microtubules to morphogenesis. *Cell* **45**, 329-342.
- LaFountain, J. R., Jr, Oldenbourg, R., Cole, R. W. and Rieder, C. (2001). Microtubule flux mediates poleward motion of acentric chromosome fragments during meiosis in insect spermatocytes. *Mol. Cell Biol.* **21**, 4054-4065.
- Ledbetter, M. C. and Porter, K. R. (1963). A "microtubule" in plant cell fine structure. *J. Cell Biol.* **19**, 239-250.
- Maddox, P., Desai, A., Oegema, K., Mitchison, T. J. and Salmon, E. D. (2002). Poleward microtubule flux is a major component of spindle dynamics and anaphase A in mitotic *Drosophila* embryos. *Curr. Biol.* **12**, 1670-1674.
- Maddox, P. S., Bloom, K. S. and Salmon, E. D. (2000). The polarity and dynamics of microtubule assembly in the budding yeast *Saccharomyces cerevisiae*. *Nat. Cell Biol.* **2**, 36-41.
- Maiato, H., Rieder, C. L. and Khodjakov, A. (2004). Kinetochore-driven formation of kinetochore fibers contributes to spindle assembly during animal mitosis. *J. Cell Biol.* **167**, 831-840.
- Mao, G., Chan, J., Calder, G., Doonan, J. H. and Lloyd, C. W. (2005). Modulated targeting of GFP-AtMAP65-1 to central spindle microtubules during division. *Plant J.* **43**, 469-478.
- Marc, J. (1997). Microtubule-organizing centres in plants. *Trends Plant Sci.* **2**, 223-230.
- Mathur, J., Mathur, N., Kernebeck, B., Srinivas, B. P. and Hulskamp, M. (2003). A novel localization pattern for an EB1-like protein links microtubule dynamics to endomembrane organization. *Curr. Biol.* **13**, 1991-1997.
- Matthies, H. J., McDonald, H. B., Goldstein, L. S. and Theurkauf, W. E. (1996). Anastral meiotic spindle morphogenesis: role of the non-claret disjunctional kinesin-like protein. *J. Cell Biol.* **134**, 455-464.
- McDonald, K. L., O'Toole, E. T., Mastronarde, D. N. and McIntosh, J. R. (1992). Kinetochore microtubules in PTK cells. *J. Cell Biol.* **118**, 369-383.
- Mitchison, T. J. (1989). Polewards microtubule flux in the mitotic spindle: evidence from photoactivation of fluorescence. *J. Cell Biol.* **109**, 637-652.
- Mitchison, T. J. (2005). Mechanism and function of poleward flux in *Xenopus* extract meiotic spindles. *Philos. Trans. R. Soc. Lond. B Biol. Sci.* **29**, 623-629.
- Mitchison, T. J. and Kirschner, M. W. (1985). Properties of the kinetochore in vitro. I. Microtubule nucleation and tubulin binding. *J. Cell Biol.* **101**, 755-765.
- Mitchison, T. J. and Salmon, E. D. (2001). Mitosis: a history of division. *Nat. Cell Biol.* **3**, E17-E21.
- Miyamoto, D. T., Perlman, Z. E., Burbank, K. S., Groen, A. C. and Mitchison, T. J. (2004). The kinesin Eg5 drives poleward microtubule flux in *Xenopus laevis* egg extract spindles. *J. Cell Biol.* **167**, 813-818.
- Niethammer, P., Bastiaens, P. and Karsenti, E. (2004). Stathmin-tubulin interaction gradients in motile and mitotic cells. *Science* **303**, 1862-1866.
- Pepper, D. A. and Brinkley, B. R. (1979). Microtubule initiation at kinetochores and centrosomes in lysed mitotic cells. Inhibition of site-specific nucleation by tubulin antibody. *J. Cell Biol.* **82**, 585-591.
- Piehl, M. and Cassimeris, L. (2003). Organization and dynamics of growing microtubule plus ends during early mitosis. *Mol. Biol. Cell* **14**, 916-925.
- Rebollo, E., Llamazares, S., Reina, J. and Gonzalez, C. (2004). Contribution of noncentrosomal microtubules to spindle assembly in *Drosophila* spermatocytes. *PLoS Biol.* **2**, E8.
- Reddy, A. S. and Day, I. S. (2001). Kinesins in the *Arabidopsis* genome: a comparative analysis among eukaryotes. *BMC Genomics* **2**, 2.
- Rieder, C. L. and Salmon, E. D. (1994). Motile kinetochores and polar ejection forces dictate chromosome position on the vertebrate mitotic spindle. *J. Cell Biol.* **124**, 223-233.
- Rieder, C. L. and Salmon, E. D. (1998). The vertebrate cell kinetochore and its roles during mitosis. *Trends Cell Biol.* **8**, 310-318.
- Rieder, C. L. and Khodjakov, A. (2003). Mitosis through the microscope: advances in seeing inside live dividing cells. *Science* **300**, 91-96.
- Rogers, G. C., Rogers, S. L., Schwimmer, T. A., Ems-McClung, S. C., Walczak, C. E., Vale, R. D., Scholey, J. M. and Sharp, D. J. (2004). Two mitotic kinesins cooperate to drive sister chromatid separation during anaphase. *Nature* **427**, 364-370.
- Rogers, G. C., Rogers, S. L. and Sharp, D. J. (2005). Spindle microtubules in flux. *J. Cell Sci.* **118**, 1105-1116.

- Ryan, K.** (1983). Chromosome movements in pollen mother cells: techniques for living cell cine-microscopy and for electron microscopy. *Mikroskopie* **40**, 67-78.
- Sharp, D. J., Rogers, G. C. and Scholey, J. M.** (2000). Microtubule motors in mitosis. *Nature* **407**, 41-47.
- Shaw, S. L., Kamyar, R. and Ehrhardt, D. W.** (2003). Sustained microtubule treadmilling in *Arabidopsis* cortical arrays. *Science* **300**, 1715-1718.
- Shirasu-Hiza, M., Perlman, Z. E., Wittmann, T., Karsenti, E. and Mitchison, T. J.** (2004). Eg5 causes elongation of meiotic spindles when flux-associated microtubule depolymerization is blocked. *Curr. Biol.* **14**, 1941-1945.
- Smirnova, E. A. and Bajer, A. S.** (1992). Spindle poles in higher plant mitosis. *Cell Motil. Cytoskeleton* **23**, 1-7.
- Smirnova, E. A. and Bajer, A. S.** (1998). Early stages of spindle formation and independence of chromosome and microtubule cycles in *Haemanthus* endosperm. *Cell Motil. Cytoskeleton* **40**, 22-37.
- Telzer, B. R., Moses, M. J. and Rosenbaum, J. L.** (1975). Assembly of microtubules onto kinetochores of isolated mitotic chromosomes of HeLa cells. *Proc. Natl. Acad. Sci. USA* **72**, 4023-4027.
- Tirnauer, J. S., Salmon, E. D. and Mitchison, T. J.** (2004). Microtubule plus-end dynamics in *Xenopus* egg extract spindles. *Mol. Biol. Cell* **15**, 1776-1784.
- Ueda, K., Matsuyama, T. and Hashimoto, T.** (1999). Visualization of microtubules in living cells of transgenic *Arabidopsis thaliana*. *Protoplasma* **206**, 201-206.
- Waters, J. C., Mitchison, T. J., Rieder, C. L. and Salmon, E. D.** (1996). The kinetochore microtubule minus-end disassembly associated with poleward flux produces a force that can do work. *Mol. Biol. Cell* **7**, 1547-1558.